Available on CMS information server

CMS CR -2009/055

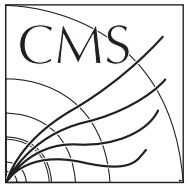

The Compact Muon Solenoid Experiment

Conference Report

Mailing address: CMS CERN, CH-1211 GENEVA 23, Switzerland

18 April 2009

Gap-Survival Probability and Rescattering in Diffraction at the LHC

Michele Arneodo[1)], Università del Piemonte Orientale, I-28100 Novara, and INFN-Torino, I-10125 Torino, Italy, on behalf of the CMS Collaboration

Abstract

The feasibility is discussed of rediscovering hard diffraction at the LHC with the first 10-100 pb^{-1} collected by the CMS detector. Studies are presented of single-diffractive di-jet production in pp collisions at $\sqrt{s} = 14$ TeV, single-diffractive W boson production and Y photoproduction. The prospects of assessing the rapidity-gap survival probability are discussed.

Presented at *International Workshop on Multiple Partonic Interactions at the LHC "1st MPI@LHC",27-31 October 2008,Perugia,Italy,16/03/2009*

[1)] speaker

Gap-Survival Probability and Rescattering in Diffraction at the LHC

Michele Arneodo[1†]
[1]Università del Piemonte Orientale, I-28100 Novara, and INFN-Torino, I-10125 Torino, Italy, on behalf of the CMS Collaboration

Abstract
The feasibility is discussed of rediscovering hard diffraction at the LHC with the first 10-100 pb^{-1} collected by the CMS detector. Studies are presented of single-diffractive di-jet production in pp collisions at $\sqrt{s} = 14$ TeV, single-diffractive W boson production and Y photoproduction. The prospects of assessing the rapidity-gap survival probability are discussed.

1 Introduction

A substantial fraction of the total proton-proton cross section is due to diffractive reactions of the type $pp \to XY$, where X, Y are either protons or low-mass states which may be a resonance or a continuum state. In all cases, the energy of the outgoing protons or the states X, Y is approximately equal to that of the incoming beam particles, to within a few per cent. The two (groups of) final-state particles are well separated in phase space and have a large gap in rapidity between them ("large rapidity gap", LRG). Diffractive hadron-hadron scattering can be described within Regge theory (see e.g. [1]). In this framework, diffraction is characterised by the exchange of a specific trajectory, the "Pomeron", which has the quantum numbers of the vacuum and notably no colour (hence the LRG).

The effort to understand diffraction in QCD has received a great boost from the seminal studies of diffractive $p\bar{p}$ collisions with the UA8 experiment at CERN [2] and more recently from studies of diffractive events in ep collisions at HERA and $p\bar{p}$ collisions at Fermilab (see e.g. [3–9] and references therein). A key to this success are factorisation theorems for ep diffractive scattering, which allow to express the cross section in terms of diffractive parton distribution functions (PDFs) and generalised parton distributions. These functions can be extracted from measurements and contain information about small-x partons that can only be obtained in diffractive processes. To describe hard diffractive hadron-hadron collisions is more challenging since factorisation is broken by rescattering between spectator partons. These rescattering effects, often quantified in terms of the so-called "rapidity-gap survival probability" [10, 11], are of interest in their own right because of their relation with multiple parton scattering.

This paper summarises some recent feasibility studies carried out by the CMS Collaboration, aiming at "rediscovering" hard-diffraction with the early LHC data and at quantifying the rapidity-gap survival probability at LHC energies by means of the single-diffractive (SD) reaction $pp \to Xp$, in which X includes either a W boson or a di-jet system. This reaction is sensitive

[†] speaker

to the diffractive structure function (dPDF) of the proton, specifically its gluon component (see e.g. [3]). It is also sensitive to the rapidity-gap survival probability, $\langle|S^2|\rangle$; to first approximation, the cross section is directly proportional to $\langle|S^2|\rangle$, independent of kinematics. This process has been studied at the Tevatron, where the ratio of the yields for SD and inclusive di-jet production has been measured to be approximately 1% [8, 12, 13]. Theoretical expectations for LHC are at the level of a fraction of a per cent [11, 14–18]. There are, however, significant uncertainties in the predictions, notably due to the uncertainty of $\langle|S^2|\rangle$. While there is some consensus that $\langle|S^2|\rangle \simeq 0.05$ [16, 17] for hard diffractive processes at LHC energies, values of $\langle|S^2|\rangle$ as low as 0.004 and as high as 0.23 have been proposed [18]. Exclusive photoproduction of Υ mesons, $pp \to p\Upsilon p$ is also briefly discussed. This reaction is sensitive to the structure of the proton, notably the generalised (or skewed) gluon density, but the rapidity-gap survival probability should in this case be close to unity [19].

The CMS apparatus is described in detail elsewhere [20]. Two experimental scenarios are considered here. In the first, no forward detectors beyond the CMS forward calorimeter HF are assumed. In this case the pseudo-rapidity coverage is limited to $|\eta| < 5$. In the second, additional coverage at $-6.6 < \eta < -5.2$ is assumed by means of the CASTOR calorimeter. HF and CASTOR are briefly discussed in the next section.

For more details on the analyses presented here, the reader is referred to [21–23].

2 The HF and CASTOR calorimeters

The forward part of the hadron calorimeter, HF, is located 11.2 m from the interaction point. It consists of steel absorbers and embedded radiation hard quartz fibers, which provide a fast collection of Cherenkov light. Each HF module is constructed of 18 wedges in a nonprojective geometry with the quartz fibers running parallel to the beam axis along the length of the iron absorbers. Long (1.65 m) and short (1.43 m) quartz fibers are placed alternately with a separation of 5 mm. These fibers are bundled at the back of the detector and are read out separately with phototubes.

CASTOR is a sampling calorimeter located at $\simeq 14$ m from the interaction point, with tungsten plates as absorbers and fused silica quartz plates as active medium. The plates are inclined by 45° with respect to the beam axis. The calorimeter has the shape of an octagonal cylinder. Particles passing through the quartz emit Cherenkov photons which are transmitted to photomultiplier tubes through air-core light-guides. The electromagnetic section is 22 radiation length deep with 2 tungsten-quartz sandwiches, and the hadronic section consists of 12 tungsten-quartz sandwiches. The total depth is 10.3 interaction lengths. The calorimeter readout has azimuthal and longitudinal segmentation (16 and 14 segments, respectively). There is no segmentation in η.

3 SD W and di-jet production

The analyses described here are planned for the first LHC data, and can be carried out on data samples with integrated luminosities of 10-100 pb^{-1} and with negligible pile-up. A centre-of-mass energy of 14 TeV is used. No near-beam proton tagger is assumed, and the selection of diffractive events has therefore to rely on the observation of a rapidity gap.

The single diffractive signals were simulated with the POMWIG Monte Carlo generator [14]. Non-diffractive events were simulated with PYTHIA [24] or MADGRAPH [25].

3.1 Event selection

3.1.1 $W \to \mu\nu$ production

The selection of the events with a candidate W decaying to $\mu\nu$ is the same as that used for inclusive $W \to \mu\nu$ production [26]. Events with a candidate muon in the pseudo-rapidity range $|\eta| > 2.0$ and transverse momentum $p_T < 25$ GeV were rejected, as were events with at least two muons with $p_T > 20$ GeV. Muon isolation was imposed by requiring $\sum p_T < 3$ GeV in a cone with $\Delta R < 0.3$. The transverse mass was required to be $M_T > 50$ GeV. The contribution from top events containing muons was reduced by rejecting events with more than 3 jets with $E_T > 40$ GeV (selected with a cone algorithm with radius of 0.5) and events with acoplanarity ($\zeta = \pi - \Delta\phi$) between the muon and the direction associated to $E_T^{\rm miss}$ greater than 1 rad.

3.1.2 Di-jet production

At the trigger level, events were selected by requiring at least 2 jets with average uncorrected transverse energy greater then 30 GeV. Offline, jets were reconstructed with the SiSCone5 [27] algorithm and jet-energy scale (JES) corrections were applied. At least two jets with $E_T > 55$ GeV were required. All plots shown in this paper are for energy-corrected jets.

3.1.3 Diffractive selection

The left panel of Fig. 1 shows the generated energy-weighted η distribution for stable particles in single-diffractive and non-diffractive W production events; only diffractive events with the scattered proton at positive rapidities (the peak at $\eta \gtrsim 10$) are included in the plot. Diffractive events have, on average, lower multiplicity both in the central region and in the hemisphere that contains the scattered proton, the so-called "gap side", than non-diffractive events. The right panel of Fig. 1 shows the multiplicity distribution in the central tracker for $|\eta| < 2$ after the di-jet selection cuts. Diffractive events have a multiplicity distribution that peaks at low values, unlike that of non-diffractive events. Diffractive event candidates were therefore selected on the basis of the multiplicity distribution in the central tracker, in the HF as well as in CASTOR.

The gap side was selected as that with lower energy sum in the HF. This selection was made for all events though the concept is relevant only for diffractive events.

In addition, for the di-jet analysis, the two leading jets were required to be between $-4 < \eta < 1$ for events with the gap side at positive rapidities and $-1 < \eta < 4$ for events with the gap side at negative rapidities. When CASTOR is used, only events with the gap on the negative side are considered, since CASTOR will be installed on that side first. The rapidity separation between the two leading jets was required to be $\Delta\eta < 3$.

Finally, a cut was applied on the track multiplicity in the central tracker. The plots shown in this paper were obtained with maximum multiplicity for $|\eta| < 2$, $N_{\rm track}^{\rm max}$, of 1, 5 and no cut at all. For the events passing this cut, multiplicity distributions in the HF and CASTOR calorimeters were studied, from which a diffractive sample can be extracted.

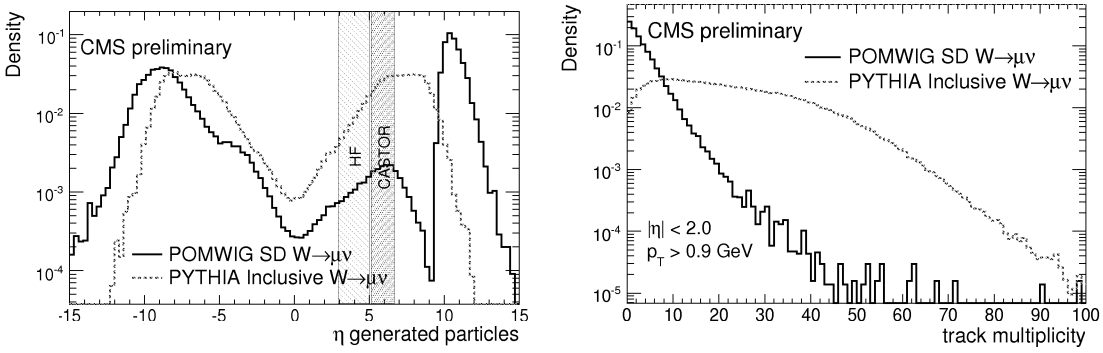

Fig. 1: Left panel: Generated energy-weighted η distribution for stable particles (excluding neutrinos) in diffractive (POMWIG, continuous line) and non-diffractive (PYTHIA, dashed line) W production events. The HF coverage and that of the CASTOR calorimeter are also shown. The diffractive events were generated with the gap side in the positive η hemisphere. The peak at $\eta \gtrsim 10$ is due to the scattered proton. The area under the histograms is normalised to unity. Right panel: Track multiplicity distribution in the central tracker after the W selection cuts for diffractive (POMWIG, continuous line) and non-diffractive (PYTHIA, dashed line) events. The track corresponding to the μ candidate is excluded. The area under the histograms is normalised to unity.

4 Results

4.1 SD $W \rightarrow \mu\nu$ production

Figure 2 shows the HF tower multiplicity for the low-η ("central slice", $2.9 < \eta < 4.0$) and high-η HF ("forward slice", $4.0 < \eta < 5.2$) regions for events with central tracker multiplicity $N_{\rm track} \leq 5$. In the figure, the top left and top right plots show the distributions expected for the diffractive W events with generated gap in the positive and negative Z direction, respectively[1]; they exhibit a clear peak at zero multiplicity. Conversely, the non-diffractive W events have on average higher multiplicities, as shown in the bottom left plot; this distribution is interesting in its own right as it is sensitive to the underlying event in non-diffractive interactions. Finally, the bottom right plot shows the sum of the POMWIG and PYTHIA distributions – this is the type of distribution expected from the data. The diffractive signal at low multiplicities is visible. The significance is highest when the $N_{\rm track}$ cut is most strict (see [21]).

The HF tower multiplicity vs CASTOR ϕ sector multiplicity was also studied for the gap side. Since CASTOR will be installed at first on the negative side of the interaction point, only events with the gap on that side (as determined with the procedure discussed above) were considered. The CMS software chain available for this study did not include simulation/reconstruction code for CASTOR; therefore, the multiplicity of generated hadrons with energy above a 10 GeV threshold in each of the CASTOR azimuthal sectors was used. Figure 3 shows plots analogous to those of Fig. 2 for the combination of HF and CASTOR. The top plots show the POMWIG distributions; the few events in the top left plot are those for which the gap-side determination was incorrect. The signal to background ratio improves greatly with respect to the HF only case since

[1]The Z axis is along the beam direction.

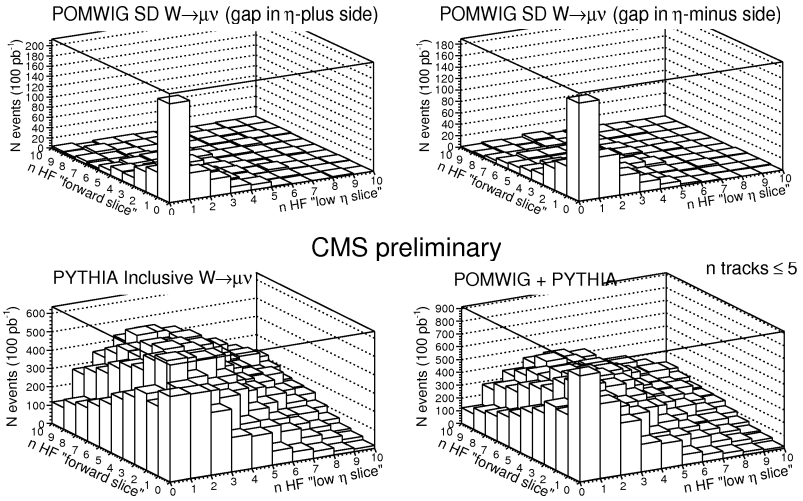

Fig. 2: Low-η ("central slice") vs high-η ("forward slice") HF tower multiplicity distributions for events with track multiplicity in the central tracker $N_{\rm track} \leq 5$. Top left: POMWIG events with gap generated in the positive Z direction. Top right: POMWIG events with gap generated in the negative Z direction. Bottom left: PYTHIA events. Bottom right: Sum of the PYTHIA and POMWIG distributions.

a wider η coverage suppresses non-diffractive events, where the gap is due to statistical fluctuations in the rapidity distribution of the hadronic final-state. Here as well, the significance is highest for small central tracker multiplicity cuts but still acceptable even when no cut is applied (see [22]). The plots also indicate that if only the CASTOR multiplicity is used, the diffractive signal is further enhanced. The accepted events with zero multiplicity in both the HF and CASTOR, i.e. the events with a candidate rapidity gap extending over HF and CASTOR and $N_{\rm track} \leq 5$, typically have $\xi \lesssim 0.01$, and thus populate the region where Pomeron exchange is expected to dominate over sub-leading exchanges. Here ξ indicates the fractional momentum loss of the proton. The ξ coverage for different $N_{\rm track}$ cuts is similar and so is that of the HF only case.

A sample of diffractive events can be obtained by using the zero-multiplicity bins, where the diffractive events cluster and the non-diffractive background is small. As an example, when an integrated effective luminosity for single interactions of 100 pb^{-1} becomes available, SD W production can then be observed with $\mathcal{O}(100)$ signal events if CASTOR is used.

4.2 SD di-jet production

Figure 4 shows the HF-only and HF vs CASTOR gap-side multiplicity distributions for different cuts on the central tracker; these plots are the equivalent of the bottom right ones of Figs. 2 and 3. The size of the enhancement in the zero-multiplicity bins relative to the rest of the distribution increases monotonically when the $N_{\rm track}^{\rm max}$ cut is tightened – the opposite of what would happen if the enhancement were a statistical fluctuation. The relative size of the enhancement also increases

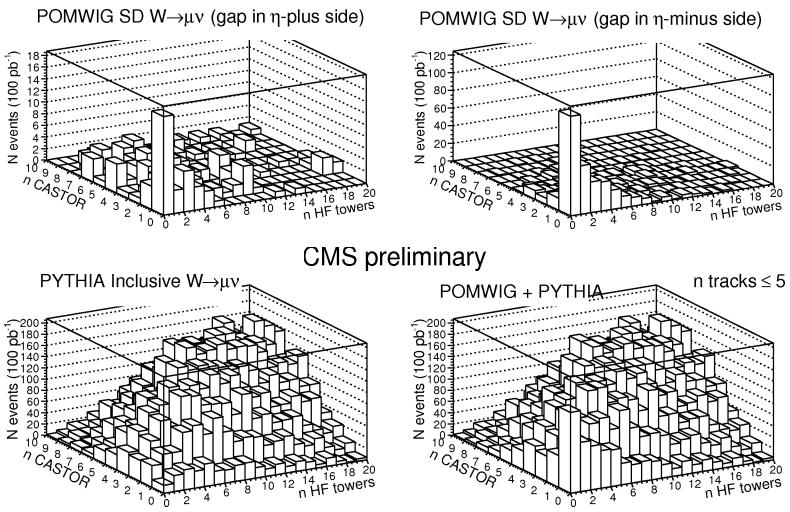

Fig. 3: HF tower multiplicity vs CASTOR sector multiplicity distribution for events with track multiplicity in the central tracker $N_{\rm track} \leq 5$. Top left: POMWIG events with gap generated in the positive Z direction (opposite side to CASTOR). Top right: POMWIG events with gap generated in the negative Z direction (same side as CASTOR). Bottom left: PYTHIA events. Bottom right: Sum of the PYTHIA and POMWIG distributions.

when going from the HF-only coverage to the HF plus CASTOR coverage: again, a wider η coverage suppresses non-diffractive events, where the gap is due to statistical fluctuations in the rapidity distribution of the hadronic final-state. Plots of this type, along with others presented in [22], can be used to demonstrate the existence of a SD di-jet signal in a data-driven, model-independent way.

Once the existence of the signal is established, here again, a sample of diffractive events can be obtained by using the zero-multiplicity bins, where the diffractive events cluster and the non-diffractive background is small. For example, when an integrated effective luminosity for single interactions of 10 pb^{-1} becomes available, SD di-jet production can then be observed with $\mathcal{O}(300)$ signal events.

4.2.1 Sensitivity to the value of the rapidity-gap survival probability

Table 1 gives the expected SD di-jet signal and background yields in the zero-multiplicity bins also for values of the rapidity-gap survival probability $\langle|S|^2\rangle = 0.004$ and $\langle|S|^2\rangle = 0.23$. In the former case, the observable signal becomes marginal, even with the widest possible η coverage (HF+CASTOR). Conversely, $\langle|S|^2\rangle = 0.23$ gives rise to a very prominent signal, also in the HF-only case.

In order to assess the significance of these yields, a preliminary, conservative estimate of the systematic uncertainties was obtained by summing in quadrature the contributions due to the sensitivity to the HF threshold ($\pm 15\%$), the jet-energy scale ($\pm 30\%$), the use of different jet algorithms ($\pm 20\%$) and a $+30\%$ contribution due to proton dissociation (see [22]), yielding a

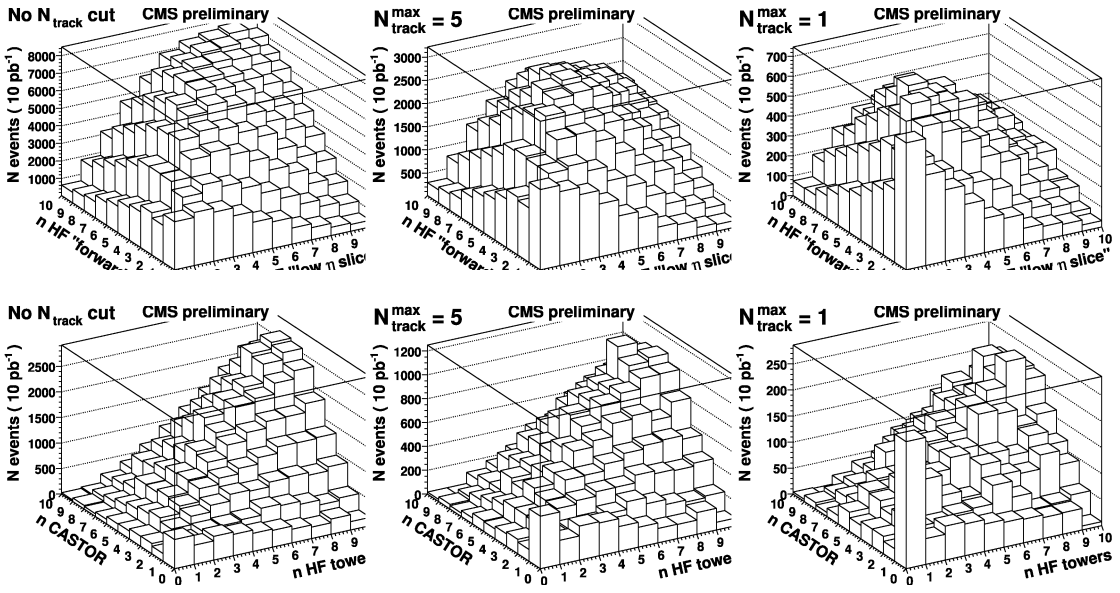

Fig. 4: HF-only (top row) and HF vs CASTOR (bottom row) multiplicity distributions for signal plus background events with no cut on the track multiplicity in the central tracker (left column), $N_{\rm track}^{\rm max} = 5$ (central column) and $N_{\rm track}^{\rm max} = 1$ (right column).

$^{+50}_{-40}\%$ systematic uncertainty.

Observation of an event yield of $236 \pm 15(\text{stat.})^{+120}_{-90}(\text{syst.})$ (cf. Table 1, $N_{\rm track}^{\rm max} = 1$ and HF+CASTOR) or $409 \pm 20(\text{stat.})^{+200}_{-160}(\text{syst.})$ (cf. Table 1, $N_{\rm track}^{\rm max} = 5$ and HF+CASTOR) would exclude $\langle |S|^2 \rangle = 0.004$, for which no signal is visible.

5 Υ photoproduction

An important term of comparison for the early determination of the rapidity-gap survival probability is exclusive Υ photoproduction, $pp \to p\Upsilon p$, in which one of the protons radiates a quasi-real photon which interacts, via colour-singlet exchange, with the other proton. This reaction has been studied at HERA, and can be investigated at CMS with the early LHC data [23]. A few hundred events events are expected in 100 pb^{-1}. This process is interesting in its own right as a window on the generalised parton distribution functions of the proton. In addition, the rapidity-gap survival probability in this case is expected to be close to unity [19]. The yield of exclusive Υ photoproduction should thus be essentially unsuppressed – and can be used to further constrain the understanding of the rapidity-gap survival probability.

6 A look at the future: near-beam proton taggers

CMS (and ATLAS [28]) will be able to carry out a forward and diffractive physics program also at the highest LHC instantaneous luminosities if the FP420 program is approved [29]. FP420 at CMS aims at instrumenting the ± 420 m region. This addition will allow measuring forward

Table 1: Diffractive and non-diffractive di-jet event yields expected with (1) zero HF multiplicity, (2) zero HF and CASTOR multiplicity, as a function of $N_{\rm track}^{\rm max}$. The signal yields are given for $\langle|S|^2\rangle = 0.05$ (nominal) as well as $\langle|S|^2\rangle = 0.004$ and $\langle|S|^2\rangle = 0.23$. The uncertainties are computed as $\sqrt{N}$.

N_{HF} = 0	$N_{\rm track}^{\rm max}$	$N_{\rm diff}$ $\langle\|S\|^2\rangle = 0.05$	$N_{\rm diff}$ $\langle\|S\|^2\rangle = 0.004$	$N_{\rm diff}$ $\langle\|S\|^2\rangle = 0.23$	$N_{\rm non-diff}$
	no cut	1047 ± 32	84 ± 9	4816 ± 69	1719 ± 41
	5	803 ± 28	64 ± 8	3694 ± 61	943 ± 31
	1	362 ± 19	29 ± 5	1665 ± 41	276 ± 16
$N_{\rm HF} = 0$, $N_{\rm CASTOR} = 0$					
	no cut	504 ± 22	40 ± 6	2318 ± 48	67 ± 8
	5	409 ± 20	33 ± 4	1881 ± 43	31 ± 6
	1	236 ± 15	19 ± 4	1086 ± 33	8 ± 3

protons with values of the fractional momentum loss of the proton $0.002 \lesssim \xi \lesssim 0.002$.

An articulate joint CMS-TOTEM research program is also foreseen [5, 30], with coverage in the region $0.02 \lesssim \xi \lesssim 0.2$, complementary to that of FP420.

7 Summary and outlook

In summary, CMS has detailed, quantitative plans to re-discover hard diffraction at LHC using rapidity gaps with the early data. The simple measurement of event yields may give early information on the rapidity-gap survival probability. Also, the shape of the background is sensitive to the underlying event in non-diffractive interactions. Once a hard-diffractive signal is established, the plan is to move on to the measurement of the ratio of diffractive to inclusive yields à la CDF and D0. Significant improvements are expected as soon as forward proton coverage becomes available via TOTEM and FP420.

References

[1] P. D. B. Collins, *An Introduction to Regge Theory and High-Energy Physics*, Cambridge University Press, Cambridge, 1977.

[2] UA8 Collaboration, A. Brandt *et al.*, Phys. Lett. B **297** (1992) 417.

[3] V. Barone and E. Predazzi, *High-energy particle diffraction*, Springer, 2002.

[4] S. Alekhin *et al.*, arXiv:hep-ph/0601013.

[5] M. Albrow *et al.*, "Prospects for diffractive and forward physics at the LHC," CERN-LHCC-2006-039, CERN-LHCC-G-124, CERN-CMS-NOTE-2007-002.

[6] M. Arneodo and M. Diehl, hep-ph/0511047 (2005).

[7] A. Solano, these Proceedings.

[8] M. Gallinaro, these Proceedings.

[9] H. Jung *et al.*, arXiv:0903.3861 [hep-ph].

[10] J. D. Bjorken, Phys. Rev. D **47** (1993) 10111;
A. B. Kaidalov *et al.*, Eur. Phys. J. C **21** (2001) 52152.

[11] L. Frankfurt, these Proceedings.

[12] F. Abe *et al.* [CDF Collaboration], Phys. Rev. Lett. **79** (1997) 2636.

[13] B. Abbott *et al.* [D0 Collaboration], Phys. Lett. B **531** (2002) 52.

[14] B. E. Cox and J. R. Forshaw, Comput. Phys. Commun. **144** (2002) 104.

[15] V. A. Khoze, A. D. Martin and M. G. Ryskin, arXiv:0802.0177 [hep-ph].

[16] E. Gotsman, E. Levin, U. Maor, E. Naftali and A. Prygarin, arXiv:hep-ph/0511060.

[17] V. A. Khoze, A. D. Martin and M. G. Ryskin, Phys. Lett. B **643** (2006) 93.

[18] J. S. Miller, Eur. Phys. J. C **56** (2008) 39.

[19] M.G. Ryskin, private communication (2008).

[20] CMS Collaboration, R. Adolphi *et al.*, JINST **3** (2008) S08004.

[21] CMS Collaboration, CMS PAS DIF-07-002 (2007).

[22] CMS Collaboration, CMS PAS FWD-08-002 (2008).

[23] CMS Collaboration, CMS PAS DIF-07-001 (2007).

[24] T. Sjostrand, S. Mrenna and P. Skands, JHEP **0605** (2006) 026.

[25] J. Alwall *et al.*, JHEP **0709** (2007) 028.

[26] CMS Collaboration, CMS PAS EWK-07-002 (2007).

[27] G. P. Salam and G. Soyez, JHEP **0705** (2007) 086.

[28] M. Campanelli, these Proceedings.

[29] The FP420 Research and Development Collaboration, M. G. Albrow *et al.*, arXiv:0806.0302 [hep-ex].

[30] F. Ferro, these Proceedings.